LIVER METASTASIS EARLY DETECTION USING FMRI BASED STATISTICAL MODEL

Moti Freiman[1], *Yifat Edrei*[2,3], *Eitan Gross*[4], *Leo Joskowicz*[1], *Rinat Abramovitch*[2,3]

[1] School of Eng. and Computer Science, The Hebrew Univ. of Jerusalem, Israel.
[2] The G. Savad Inst. for Gene Therapy, Hadassah Hebrew University Medical Center, Jerusalem, Israel.
[3] MRI/MRS lab HBRC, Hadassah Hebrew University Medical Center, Jerusalem, Israel.
[4] Pediatric Surgery, Hadassah Hebrew University Medical Center, Jerusalem, Israel.

Email: freiman@cs.huji.ac.il

ABSTRACT

We present a novel method for computer aided early detection of liver metastases. The method used fMRI-based statistical modeling to characterize colorectal hepatic metastases and follow their early hemodynamical changes. Changes in hepatic hemodynamics were evaluated from T_2*-W fMRI images acquired during the breathing of air, air-CO_2, and carbogen. A classification model was built to differentiate between metastatic and healthy liver tissue. The model was constructed from 128 validated fMRI samples of metastatic and healthy mice liver tissue using histogram-based features and SVM classification engine. The model was subsequently tested with a set of 32 early, non-validated fMRI samples. Our model yielded an accuracy of 84.38% with 80% precision.

Index Terms— Liver metastasis, fMRI analysis, early detection, statistical analysis, computer-aided diagnosis

1. INTRODUCTION

The liver is the second most commonly involved organ in metastatic disease, after the lymph nodes. It is the most common site of visceral metastases for colorectal carcinoma patients, and hepatic metastases are a frequent clinical complication. Some focal lesions may be surgically resectable or treated by means of ablation techniques. Since liver function tests in patients with liver metastases tend to be insensitive and non-specific, the disease is usually diagnosed at later stages. Despite the availability of numerous possible treatments, hepatic metastases are difficult to eradicate because of their late discovery. Early and accurate detection of these lesions is recognized as having the potential of improving survival rates and reducing treatment morbidity.

A key observation is that there are changes in liver blood supply that can serve as an indicator for the presence of hepatic metastases [1]. It is well known that, whereas normal liver is supplied predominantly by the portal vein, in patients with overt colorectal liver metastases, a higher proportion of liver blood flow is derived from the hepatic artery. Thus, by monitoring hemodynamical changes, earlier detection of hepatic metastases may be feasible.

Imaging plays a central role in the early diagnosis of liver metastases. The association between hepatic metastases and altered liver blood flow has been demonstrated recently by dynamic scintigraphy [1], by Doppler sonography [2, 3], by dynamic contrast enhanced CT [4] and more recently by dynamic contrast enhanced MRI [5]. Measurements using MRI can potentially overcome limitations posed by other imaging techniques, such as poor spatial resolution in radionuclide studies, lack of reproducibility in Doppler US and radiation exposure using CT. Currently, acquisition of perfusion images in both CT and MRI require the intravenous administration of a contrast agent. Good separation of arterial from portal phase requires high temporal resolution which enforces reduction of the spatial resolution.

In a previous work [6], we demonstrated the feasibility of fMRI with hypercapnia and hyperoxia for monitoring changes in liver perfusion and hemodynamics without the need of a contrast agent administration. Using this method we characterized colorectal hepatic metastases and were able to follow their early hemodynamical changes [7, 8]. Since our method detects steady state levels without the use of contrast agent there is no need to compromise the spatial resolution and image quality. Therefore, we expect to be able to detect smaller lesions. However, the manual analysis of the hemodynamical maps produced by this method turned out to be a difficult, time consuming, and potentially unreliable task.

In this work we present a machine learning approach for the automatic detection of colorectal hepatic metastases based on their hemodynamical changes. First, we construct a statistical model describing the hemodynamical changes of colorectal hepatic metastases from samples obtained at advanced phase of metastases growth, where the metastases were visible in the anatomical MRI. Then, new samples obtained at the earlier phase of metastases growth, where the metastases are not yet visible in the anatomical image, are classified ac-

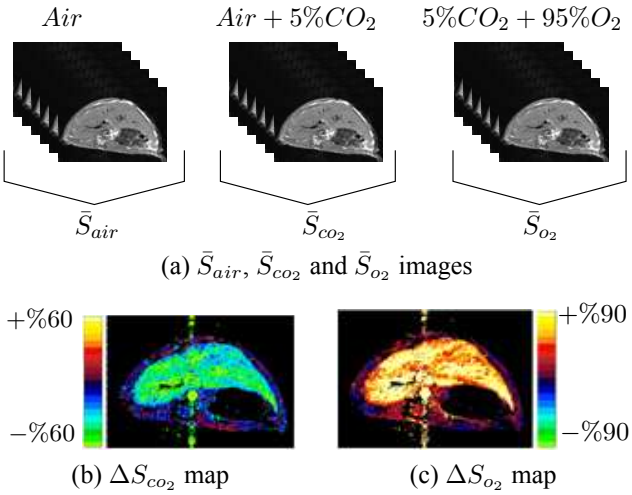

(a) $\bar{S}_{air}$, $\bar{S}_{co_2}$ and $\bar{S}_{o_2}$ images

(b) ΔS_{co_2} map (c) ΔS_{o_2} map

Fig. 1. (a) Maps of mean signal intensity values for each pixel acquired during the different inhaled gases ($\bar{S}_{air}$, $\bar{S}_{co_2}$ and $\bar{S}_{o_2}$) calculated for each gas from several repeats; (b,c) Percentage of change of fMRI signal induced by hypercapnia (ΔS_{co_2}, b) and hyperoxia (ΔS_{o_2}, c) as computed with Eqs. 1 and 2. Data is presented as color maps as indicated in the color bars.

cording to the model. Suspected areas of metastases are then enhanced in the fMRI images. We expect that this method will help radiologists to highlight undetectable metastases in a much earlier stage, with increased diagnostic specificity and sensitivity.

2. METHOD

2.1. MRI data acquisition

The input data consists of four types of images: anatomical MRI images, and three types of fMRI images of the hepatic hemodynamics. They are all acquired following the protocol described in [6]. The fMRI images are acquired during the breathing of air, air-CO_2 (5% CO_2), and carbogen (95% oxygen; 5% CO_2). Maps of mean signal intensity values for each pixel during the different inhaled gases are calculated from 6 repeats for each gas. (Fig. 1a). The percentage of change of fMRI signal intensity induced by hypercapnia (ΔS_{co_2}, Fig. 1b) and hyperoxia (ΔS_{o_2}, Fig. 1c) are calculated using the following equations:

$$\Delta S_{co_2} = \frac{\bar{S}_{co_2} - \bar{S}_{air}}{\bar{S}_{air}} \times 100 \quad (1)$$

$$\Delta S_{o_2} = \frac{\bar{S}_{o_2} - \bar{S}_{co_2}}{\bar{S}_{co_2}} \times 100 \quad (2)$$

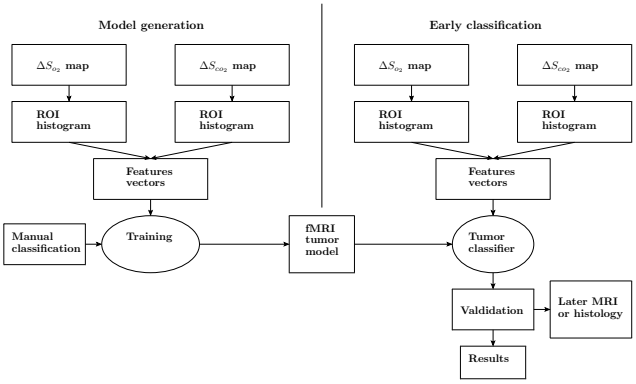

Fig. 2. Method flowchart: model generation and early classification.

2.2. Automatic classification

We use a machine-learning approach for the automatic classification of metastases using these images. Our approach consists of two stages. In the first stage we construct a statistical model from a training dataset of anatomical and fMRI images with confirmed tumors. In the second stage, we use this model to classify new fMRI images obtained at earlier phase of metastases growth. Fig. 2 summarizes in a flowchart the steps of each stage, which we explain in detail below.

2.3. Model generation

The input training set for model generation consists of a series of datasets from live subjects with and without metastases. Each dataset consists of an anatomical MRI image as well as ΔS_{co_2} and ΔS_{o_2} maps computed with Eqs. 1 and 2.

For each ΔS_{co_2} and ΔS_{o_2} image map, one or more square Regions of Interest (ROIs) containing tumors are manually identified according to the anatomical image. Each region is described by a features vector consisting of two histogram vectors, one for each map. Each histogram vector is the normalized one-dimensional histogram of the intensity values in the ROI with a fixed number of bins of equal size. These features vectors show better performance that the actual pixel vectors, as they can cope with varying tumor sizes.

Each region is classified by expert observer as either healthy (Fig. 3a) or metastasis (Fig. 3d) according to the anatomical MRI image. The corresponding features-vectors are then computed from the ΔS_{co_2} and ΔS_{o_2} maps (Fig. 3b,c for healthy tissue, and Fig. 3e,f for confirmed metastatic tissue).

A Support Vector Machine (SVM) classification engine [9] trained with this training set is then applied. It uses a generalized Radial Basis Function (RBF) kernel with the Earth Movers Distance (EMD) [10] as the affinity measure:

$$K_{emd} = e^{-emd(h_1,h_2)} \quad (3)$$

where emd is the EMD distance between the two histograms (h_1, h_2). Since the histograms are one-dimensional, the EMD distance is the L^1 norm between the cumulative histograms.

2.4. Early classification

The ΔS maps of additional subjects are acquired during the early metastases growth phase, which no metastases are visible in the anatomical images (T_2W). The ROIs and their corresponding features-vectors are computed as described in the model generation phase. The features-vectors are then classified based on the generated metastasis classification model.

2.5. Diagnosis support system

An automatic diagnosis support system for metastatic regions enhancement in fMRI images uses the proposed model. For each set of fMRI maps, (ΔS_{co_2} and ΔS_{o_2}), the system identifies regions whose features-vectors are similar to the metastases samples in the model, and then enhances them for improved visualization. The region search proceeds as follows. First, the images are thresholded with an experimentally set value to reduce the number of suspected pixels. Then, for each pixel above the threshold value, several features-vectors of its neighborhoods are build. Neighborhoods of various sizes are used to facilitate the detection of suspected regions in different stages of the metastasis development. The features-vectors are then classified with the generated model. Finally, the suspected regions are marked, so that the radiologist can then carefully evaluate these regions and decide on the appropriate follow-up.

3. EXPERIMENTAL RESULTS

3.1. MRI data acquisition

We performed an animal study on CB6F1 mice that underwent splenic injection with CT-26 colon cancer cells (10^4 cells/mouse in 0.3ml) to generate metastases. The spleen was removed 5 minutes later. In this model, 1-5 hepatic nodules were detected 13-15 days after cell inoculation by using T_2W fast SE. Metastases progression was monitored twice a week by MRI. When metastases reached to large size, animals were sacrificed, and livers were taken for histology. MRI scans were performed on a 4.7T Bruker Biospec spectrometer with a bird cage coil. Metastases assessment was done using T_2-weighted fast SE images (TR/TE=2000/40ms). Changes in hepatic hemodynamics were evaluated using T_2*-weighted GE (TR/TE=147/10ms). Images were acquired during breathing of air, air-CO_2 (5% CO_2), and carbogen (95% oxygen; 5% CO_2). A detailed description of the acquisition protocol is provided in [6].

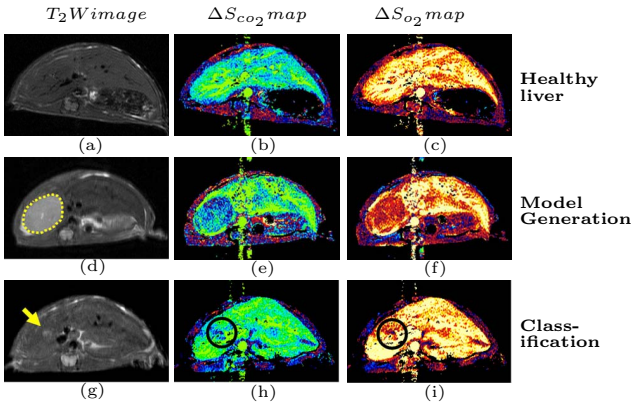

Fig. 3. Representative T_2W anatomical images (left), ΔS_{co_2} maps (center) and ΔS_{o_2} maps (right) of mice livers Healthy liver (a-c); Confirmed metastatic region (d, yellow circle) from late phase growth (21 days following cell injection) that was taken for model generation (d-f); Suspected area (g, yellow arrow) from early phase growth (14 days following cell injection) that was taken for classification. Note typical changes in the corresponding ΔS maps (encircled area in h and i).

3.2. Computer aided analysis

A SVM based classification model was generated from a database consisting of 128 samples of ΔS_{co_2} and ΔS_{o_2} maps with 64 samples of confirmed metastatic regions and 64 samples of healthy livers. The model was generated using a SVM engine implemented with an EMD based kernel [11]. We validated the consistency of our model with the "leave-one-out" technique on ΔS_{co_2} alone, ΔS_{o_2} alone, and both ΔS_{co_2} and ΔS_{o_2}. The best results were obtained with the ΔS_{co_2} features: 6.77% error and 94.03% precision.

Then, 32 samples of ΔS maps that were acquired during the early metastases growth phase were classified. In all of those samples, there were no visible metastases in the anatomical images (T_2-weighted) at that point in time (between days 10-15 after metastases cells injection). Out of the 32 samples, 11 were confirmed as metastases at later time points using anatomical images of the same position, and 21 samples showed a healthy liver. Out of these 21 negative samples, 9 samples had "metastatic-like" ΔS maps when observed with the naked eye. All 32 samples were classified according to the generated model and validated later by MRI or by histology. Our model achieved 84.38% accuarcy, 80% precision, and 72.73% recall. These results are better than the "naked eye" decisions regarding metastases existence at early time points, where metastases are not detectable in anatomical images.

The diagnosis support system automatically inspected the fMRI slices and enhanced suspicious regions based on the generated model. Representative results are shown in Fig. 4.

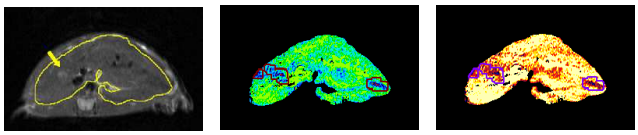

(a) Anatomical image (b) ΔS_{co_2} map (c) ΔS_{o_2} map

Fig. 4. Representative example of automatic metastases diagnosis. (a) Anatomical image, (b) ΔS_{co_2} map, (c) ΔS_{o_2} map of mouse liver with suspected metastases (yellow arrow in a); ΔS values as indicated in the color bar in Fig. 1. Computer analysis results of "metastatic-like" regions (encircled areas in b and c) included the suspected region in a.

4. CONCLUSION

This paper presents a novel method and system for early detection of liver metastases using computerized analysis of fMRI images. The analysis uses histogram-based features-vectors and an SVM classifier to produce a tumor model.

Our results indicate that histogram-based features are a useful tool for computerized analysis of fMRI images. These features have lower dimensionality than the pixels themselves, are less sensitive to the position of the fMRI response in the sample, and are invariant to the diameter of the sample due to normalization of the histogram by the total number of pixels for each sample. Our classification method yields better results than the "naked eye" decisions regarding metastases existence at early time points, where metastases are not detectable in anatomical images. The classification accuracy is high (84.38%) and the number of false-positive samples is much lower than using manual analysis (2 vs. 9 samples with the model vs. human inspection).

In the future, we will explore methods for completely automatic detection of metastases using their actual ROIs instead of rectangular ones, using higher-level features, and advanced classification techniques. We also plan to improve the results with larger training and testing datasets.

5. REFERENCES

[1] S.H. Leveson, P.A. Wiggins, G.R. Giles, A. Parkin, and P.J. Robinson, "Deranged blood flow patterns in the detection of liver metastases," *British J. of Surgery*, vol. 72, pp. 128–130, February 1985.

[2] E. Leen, J.A. Goldberg, J. Robertson, W.J. Angerson, G.R. Sutherland, T.G. Cooke, and C.S. McArdle, "Early detection of occult colorectal hepatic metastases using duplex colour Doppler sonography," *British J. of Surgery*, vol. 80, pp. 1249–1251, October 1993.

[3] S.D. Yarmenitis, C.P. Kalogeropoulou, O. Hatjikondi, P. Ravazoula, T. Petsas, D. Siamblis, and F. Kalfarentzos, "An experimental approach of the Doppler perfusion index of the liver in detecting occult hepatic metastases: histological findings related to the hemodynamic measurements in Wistar rats," *European Radiology*, vol. 10, no. 3, pp. 417–424, February 2000.

[4] C.A. Cuenod, I. Leconte, N. Siauve, A. Resten, C. Dromain, B. Poulet, F. Frouin, O. Clement, and G. Frija, "Early changes in liver perfusion caused by occult metastases in rats: Detection with quantitative CT," *Radiology*, vol. 218, no. 2, pp. 556–561, 2001.

[5] J.J. Totman, R.L. O'Gorman, P.A. Kane, and J.B. Karani, "Comparison of the hepatic perfusion index measured with gadolinium-enhanced volumetric MRI in controls and in patients with colorectal cancer," *British J. of Radiology*, vol. 78, no. 926, pp. 105–109, 2005.

[6] H. Barash, E. Gross, I. Matot, Y. Edrei, G. Tsarfaty, G. Spira, I. Vlodavsky, E. Galun, and R. Abramovitch, "fMRI during hypercapnia and hyperoxia: a non-invasive monitoring tool for changes in liver perfusion and hemodynamics in a rat model," *Radiology*, vol. 243, no. 3, pp. 727–735, 2007.

[7] Y. Edrei, E. Gross, E. Pikarsky, E. Galun, and R. Abramovitch, "Characterization and early detection of liver metastasis by fMRI," Proc. 14th Int. Society of Magnetic Resonance in Medicine (ISMRM) Scientific Meeting, May 2006, Abstract no. 1752.

[8] M. Freiman, Y. Edrei, E. Gross, L. Joskowicz, and R. Abramovitch, "Computer assisted early detection of liver metastases from fMRI maps," in *21th Int. Conf. on Computer Assisted Radiology and Surgery*. CARS, 2007, Elsevier.

[9] V.N. Vapnik, *The nature of statistical learning theory*, Springer-Verlag, Inc., NY, USA, 1995.

[10] Y. Rubner, C. Tomasi, and L.J. Guibas, "A metric for distributions with applications to image databases," in *6th Int. Conf. on Computer Vision*. ICCV, 1998, pp. 59–66.

[11] J. Thorsten, "Making large-scale support vector machine learning practical," in *Advances in kernel methods: support vector learning*, B. Schölkopf et al., Ed., pp. 169–184. MIT Press, Cambridge, MA, USA, 1999.